NANO LETTERS

2009
Vol. 9, No. 11
3801-3804

Near-Field Imaging with a Localized Nonlinear Light Source

Stefano Palomba and Lukas Novotny*

Institute of Optics, University of Rochester, Rochester, New York 14627

Received June 22, 2009; Revised Manuscript Received August 4, 2009

ABSTRACT

We demonstrate high-resolution near-field imaging and spectroscopy using the nonlinear optical response of a gold nanoparticle pair as an excitation photon source. Femtosecond pulses of frequencies ω_1 and ω_2 are used to induce a nonlinear polarization at the four wave mixing (4WM) frequency $2\omega_1 - \omega_2$ in the junction of the nanoparticle dimer. The nonlinear response leads to localized photon emission, which is employed as an excitation source for fluorescence and extinction imaging. The principle of this imaging technique is demonstrated for samples of fluorescent nanospheres and tubular J-aggregates.

Because of the wave nature of light, it is not possible to focus light to length scales smaller than roughly one-half of the wavelength using propagating radiation.[1,2] Despite this limitation it has been recently demonstrated that the diffraction limit can be overcome in fluorescence imaging.[3−7] These techniques make use of the a priori known photophysical properties of the molecules to be imaged, which is not applicable to spectroscopic techniques such as infrared absorption, Raman scattering, or coherent anti-Stokes Raman scattering (CARS).[8] In general, any form of prior information about the sample to be imaged can be used to improve the spatial resolution.

In near-field optics, the diffraction limit is circumvented by allowing nonpropagating evanescent fields to participate in the light-matter interaction.[9] Evanescent fields increase the bandwidth of spatial frequencies and make it possible to localize optical fields to length scales much smaller than half of the wavelength. However, to access evanescent fields requires that the source (e.g., aperture or scatterer) be placed very close to the sample to be imaged. As a consequence, the resulting images reflect the probe-sample interaction strength and not necessarily the properties of the sample. However, near-field optical imaging does not rely on a priori knowledge of sample properties, which makes it a valuable tool for high-resolution spectroscopic imaging.[10,11]

To ensure a strong near-field interaction it is desirable to employ an optical antenna to concentrate incoming radiation on the sample to be imaged.[12−17] By reciprocity, the optical antenna also helps to effectively reradiate the optical response due to the near-field interaction.[18] In the simplest case, the optical antenna consists of a single gold nanoparticle.[19−22] While the efficiency of a nanoparticle antenna is limited, it has the advantage of being an experimentally reproducible geometry and being describable by a simple theoretical model.[23]

It has been shown that gold nanoparticles give rise to a strong third-order nonlinear response.[24,25] For configurations consisting of multiple nanoparticles the nonlinear response depends sensitively on geometric variations, such as on the gap of a nanoparticle dimer.[25−27] We have recently demonstrated that a plasmonic dimer generates efficient four-wave mixing at the junction[17] and that it constitutes a highly confined tunable photon source. Here we use the nonlinear response of a gold nanoparticle dimer for near-field optical imaging. Photons at the four-wave mixing (4WM) frequency $\omega_{4WM} = 2\omega_1 - \omega_2$ (ω_1 and ω_2 being the frequencies of external laser radiation) are highly localized, coherent, and frequency tunable. We demonstrate high-resolution fluorescence imaging by tuning ω_{4WM} into the absorption spectrum of fluorescent sample molecules. This type of near-field imaging is essentially background-free since the sample produces no 4WM signal.

As illustrated in Figure 1, we attach a gold nanoparticle dimer to the end of a pointed optical fiber. The fabrication of these dimer antennas follows several sequential steps. First, a pulled fiber is cleaned in an oxygen plasma, then it is functionalized with (3-aminopropyl)trimethoxysilane (APTMES) at ∼80−90° to enable Au particle adhesion to the glass. The fiber is then mounted onto a quartz tuning fork for later feedback control.[22] The tuning fork with attached fiber tip is used in a shear-force microscope to image a sample with dispersed 80 nm gold nanoparticles. Once a single nanoparticle has been identified, the feedback loop is deactivated and the functionalized fiber tip is gently pressed against the particle to establish chemical bonding between the APTMES functionalized glass fiber and the Au particle.

* To whom correspondence should be addressed. E-mail: www.nano-optics.org.

10.1021/nl901986g CCC: $40.75
Published on Web 08/21/2009

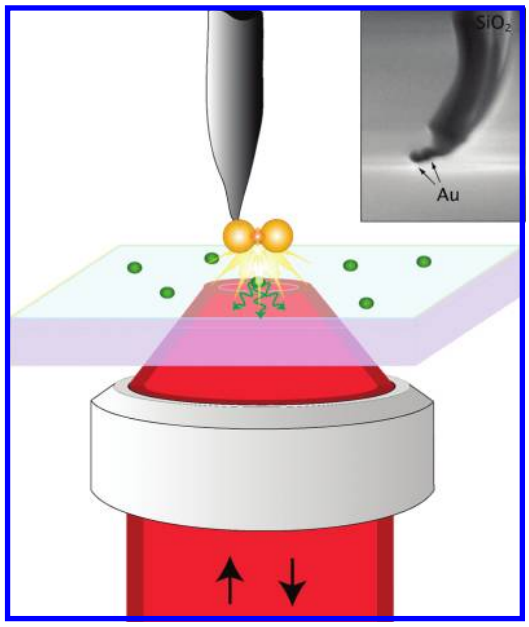

Figure 1. Illustration of the experiment. A gold nanoparticle dimer attached to a sharply pointed optical fiber serves as a nonlinear photon source. The nanoparticle dimer is excited by two incident laser beams of frequencies ω_1 and ω_2, giving rise to four-wave mixing (4WM) at frequency $\omega_{4WM} = 2\omega_1 - \omega_2$ generated at the nanoparticle junction. This localized source of radiation is used as a fluorescence excitation source for the sample placed underneath. A near-field fluorescence image is generated by raster scanning the sample and detecting pixel by pixel the emitted fluorescence. Inset: Electron micrograph of a nanoparticle dimer probe.

The resulting single-nanoparticle probe is then used to reimage the sample surface in order to identify and pick up a second gold nanoparticle. In the next step, we locally irradiate the fabricated dimer antenna with laser pulses of center frequency ω_1 and ω_2, respectively, and monitor the spectrum of the emitted radiation. This procedure helps us to identify suitable dimer antennas for subsequent near-field optical imaging; we retain only antennas that yield a strong third-order response at $\omega_{4WM} = 2\omega_1 - \omega_2$ and a negligible second-order response at $2\omega_1$, $2\omega_2$, and $\omega_1 + \omega_2$. A weak second-order response is indicative for a symmetric dimer antenna because of its point-symmetry. Representative spectra of the emitted radiation are shown in Figure 2 for two different dimer antennas. In (a) the second-order nonlinear response is clearly recognizable, whereas in (b) it is greatly suppressed.

The laser pulses are generated by a Ti:Sapphire laser providing pulses of duration ~200 fs, repetition rate of ~76 MHz, and tunable wavelength of $\lambda_1 = 740-821$ nm. This laser also pumps an optical parametric oscillator (OPO) providing pulses of the same duration, and tunable wavelength of $\lambda_2 = 1078 - 1170$ nm. A delay line is used to adjust the time difference between the two excitation pulses. Nonlinear four-wave mixing can be generated only when the two exciting laser pulses are overlapping in time and space.

As illustrated in Figure 1, an objective with numerical aperture NA = 1.3 is used to focus both laser beams on the surface of a quartz slide, which supports the sample to be imaged. The average input powers for Ti:Sapphire laser and OPO are ~10−20 μ W and ~0.5 mW, respectively.

To determine the required excitation power levels, we used a sample with monodispersed red fluorescent nanospheres of 40 nm diameter. The absorption spectrum of the nanospheres has a maximum at ~660 nm and the corresponding fluorescence spectrum peaks at ~680 nm. To excite the nanospheres, we tune the four-wave mixing frequency to $\lambda_{4WM} = 630$ nm (c.f. Figure 2b). The dimer antenna is positioned into the focii of the stationary excitation beams, and the sample with the nanospheres is raster scanned underneath the dimer antenna while detecting the fluorescence in the wavelength range of [694−738] nm. Simultaneously, we record the topography of the sample by monitoring the vertical motion of the particle dimer antenna during shear-force feedback.

Figure 3 shows a sequence of images of the same sample area. Panels a−d are optical images that have been recorded sequentially. Panel e is the corresponding topography demonstrating that each fluorescent nanosphere traces out the characteristic profile of the dimer antenna. The excitation intensity of the laser beams ω_1 and ω_2 was gradually increased from panel a to panel d. For low excitation intensities, the optical contrast is dominated by extinction of the two-photon luminescence (TPL) continuum[28] emitted from the laser-irradiated dimer antenna. This continuum is very weak in the spectra shown in Figure 2 because high excitation intensities have been used.

For weak intensities, the ratio of 4WM to TPL is small, which explains the dominance of extinction due to the continuum. The TPL contribution spans over the entire detection window giving rise to double-lobed extinction patterns. These double-lobe patterns indicate that the excited TPL signal is not entirely localized at the dimer junction, but that it spreads over the entire dimer.

We gradually increase the excitation power until the emitted fluorescence overcomes the TPL background generated by the dimer antenna. It is evident from Figure 3d that the fluorescence is strongest when the dimer junction is centered over a nanosphere. The excitation fields and the 4WM intensity are strongest at the junction. Furthermore, it can be expected that fluorescence quenching is weakest near the junction of the dimer. Our results demonstrate that 4WM at the junction of a dimer antenna defines a highly localized and effective fluorescence excitation source. The fluorescence excitation can also be temporally controlled by varying the temporal overlap between the excitation pulses. Introducing a small time delay makes the fluorescence emission disappear.

Having determined the required excitation power levels (10−20 and 500 μW for Ti:Sapphire and OPO, respectively) we now apply the imaging technique to a sample of J-aggregates. The sample is prepared by depositing a 5−10 nm poly(methyl methacrylate) (PMMA) layer on a glass substrate and then spin-casting a double-walled tubular J-aggregate solution.[29] Figure 4a shows a typical absorption spectrum of the J-aggregate solution. To maximize the excitation efficiency, we tune the 4WM frequency to λ_{4WM}

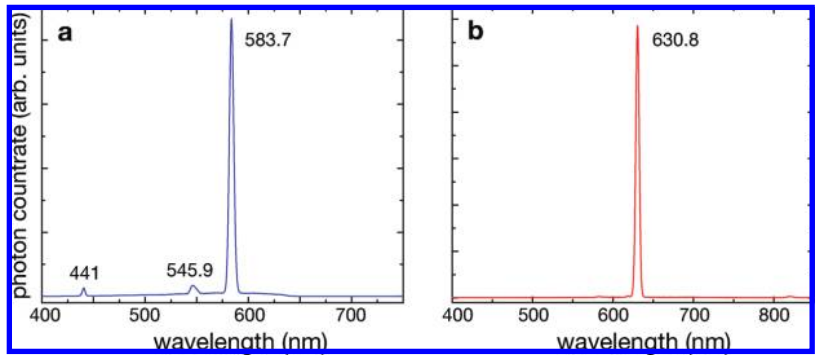

Figure 2. Spectra of photons emitted from a ~80 nm symmetrical particle dimer excited by laser pulses of center frequency ω_1 and ω_2. (a) Spectrum corresponding to $\lambda_1 = 765$ nm and $\lambda_2 = 1105$ nm, respectively. Four-wave mixing at the dimer junction gives rise to photon emission at $\lambda_{4WM} = 584$ nm. The smaller peaks correspond to residual second-order processes. (b) Spectrum from a highly symmetric nanoparticle dimer recorded for $\lambda_1 = 821$ nm and $\lambda_2 = 1170$ nm. The second-order response is completely suppressed.

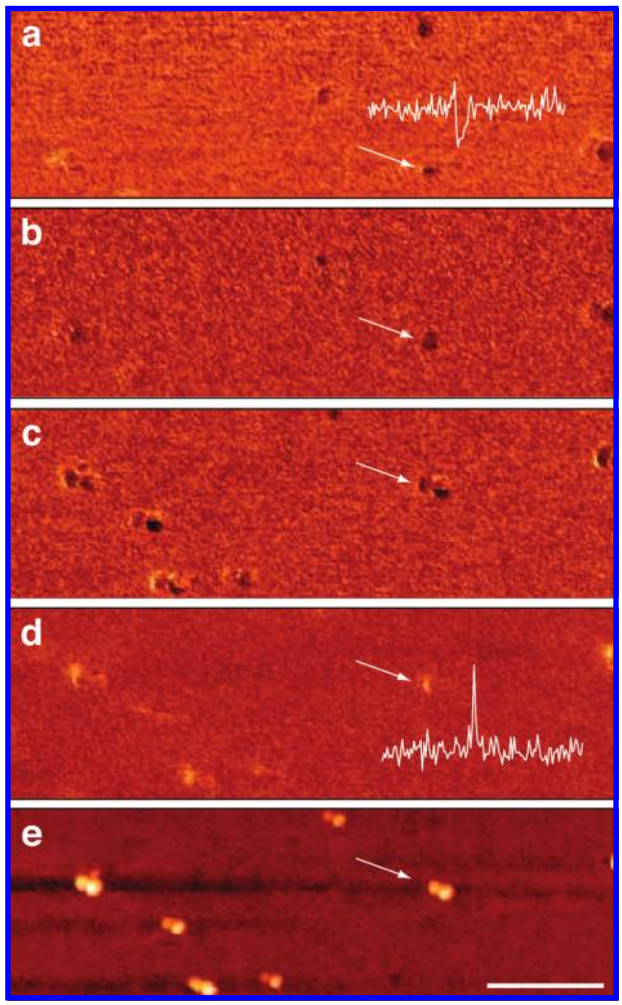

Figure 3. Contrast from 40 nm fluorescent nanospheres as a function of excitation intensity. All images show the same sample region. The powers of the laser ω_1 and ω_2 has been continuously increased from (a−d). The topographic image (e) shows that each nanosphere traces out the characteristic shape of the dimer antenna. At low excitation powers, the contrast is dominated by extinction of two-photon luminescence originating from the dimer antenna. At higher excitation powers the contrast is defined by fluorescence emission from the nanospheres. The fluorescence is at a maximum when the nanosphere faces the junction of the dimer antenna. The insets show cross sections through the nanosphere indicated by the arrows. Scale bar: 600 nm.

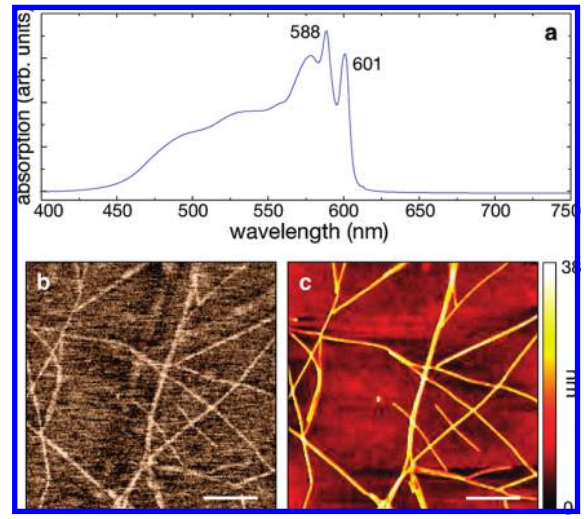

Figure 4. Near-field imaging of double-walled tubular J-aggregates. (a) Absorption spectrum of the J-aggregate solution used. (b) Near-field image recorded with a dimer antenna emitting at $\lambda_{4WM} = 584$ nm. The contrast in the image corresponds to the integrated photon counts in the wavelength range [610−623] nm. (c) Simultaneously recorded topographic image. Scale bar: 600 nm.

= 584 nm such that it coincides with one of the absorption peaks of the J-aggregates. We then raster-scan the sample underneath the laser-irradiated dimer antenna using the shear-force control described earlier. Figure 4b,d shows the simultaneously recorded fluorescence and topographic images. The optical detection window has been set to [610−623] nm, which captures most of the emitted fluorescence and effectively suppresses the 4WM excitation. By temporally separating the two excitation peaks, the optical signal becomes considerably weaker. A residual background survives because of TPL and also due to residual second-order processes (c.f. Figure 2b). Notice, that the 4WM excitation scheme not only depends on the temporal and spatial overlap of the excitation pulses but also on the their polarization. Effective 4WM requires that the excitation fields are polarized along the dimer axis.[25]

In conclusion, we have demonstrated that the nonlinear response at a gold nanoparticle junction defines a localized, tunable, and narrow-band photon source, which can be

employed for high-resolution fluorescence imaging. Since the wavelength of the 4WM signal can be tuned over a wide spectral range, the plasmonic dimer is also ideally suited for local extinction measurements. Because of broadband TPL, we are able to observe fluorescence only for excitation intensities above a certain threshold. Additionally, the emitted fluorescence can be turned on and off by controlling the temporal overlap between the excitation pulses. Moreover, the 4WM can be tuned into the absorption band of fluorescent molecules. We anticipate that the ability of switching on and off localized photon sources will find applications in nanophotonics and in active plasmonics.

Acknowledgment. The authors thank Palash Bharadwaj and Christiane Höppener for support in optical antenna fabrication. This work was supported by NSF (Grant ECCS-0651079) and AFOSR (Grant F-49620-03-1-0379, MURI).

References

(1) Abbe, E. *Archiv f. Miroskop. Anat.* **1873**, *9*, 413.
(2) Rayleigh, L. *Phil. Mag.* **1879**, *8*, 261–486.
(3) Dyba, M.; Hell, S. *Phys. Rev. Lett.* **2002**, *88*, 163901.
(4) K, I; Willig, S. O; Rizzoli, V. W. R. J.; Hell, S. W. *Nature* **2006**, *440*, 935–939.
(5) Rust, M. J.; Bates, M.; Zhuang, X. *Nat. Methods* **2006**, *3*, 793.
(6) Betzig, E.; Patterson, G. H.; Sougrat, R.; Lindwasser, O. W.; Olenych, S.; Bonifacino, J. S.; Davidson, M. W.; Lippincott-Schwartz, J.; Hess, H. F. *Science* **2006**, *313*, 1642–1645.
(7) Hess, S. T.; Girirajan, T. P.; Mason, M. D *Biophys. J.* **2006**, *91*, 4258–4272.
(8) Zumbusch, A.; Holtom, G.; Xie, X. *Phys. Rev. Lett.* **1999**, *82*, 4142–4145.
(9) Novotny, L.; Hecht, B. *Principles of Nano-Optics*; Cambridge University Press: Cambridge, 2006.
(10) Knoll, B.; Keilmann, F. *Nature* **1999**, *399*, 134.
(11) Hartschuh, A.; Beversluis, M. R.; Bouhelier, A.; Novotny, L. *Phil. Trans. R. Soc. London, Ser. A* **2003**, *362*, 807–819.
(12) Novotny, L.; Sanchez, E. J.; Xie, X. S. *Ultramicroscopy* **1998**, *71*, 21–29.
(13) Farahani, J. N.; Pohl, D. W.; Eisler, H.-J.; Hecht, B. *Phys. Rev. Lett.* **2005**, *95*, 017402.
(14) Novotny, L.; Stranick, S. J. *Annu. Rev. Phys. Chem.* **2006**, *57*, 303–331.
(15) Alda, J.; Rico-García, J.; López-Alonso, J.; Boreman, G. *Nanotechnology* **2005**, *16*, S230–S234.
(16) Taminiau, T. H.; Stefani, F. D.; Segerink, F. B.; van Hulst, N. F. *Nat. Photon.* **2008**, *2*, 234–237.
(17) Palomba, S.; Danckwerts, M.; Novotny, L. *J. Opt. A: Pure and Appl. Opt.*, submitted for publication, **2009**.
(18) Carminati, R.; Nieto-Vesperinas, M.; Greffet, J.-J. *J. Opt. Soc. Am. A* **1998**, *15*, 706–712.
(19) Fischer, U. C.; Pohl, D. W. *Phys. Rev. Lett.* **1989**, *62*, 458–461.
(20) Anger, P.; Bharadwaj, P.; Novotny, L. *Phys. Rev. Lett.* **2006**, *96*, 113002.
(21) Küehn, S.; Hakanson, U.; Rogobete, L.; Sandoghdar, V. *Phys. Rev. Lett.* **2006**, *97*, 017402.
(22) Höppener, C.; Novotny, L. *Nano Lett.* **2008**, *8*, 642–646.
(23) Bharadwaj, P.; Novotny, L. *Opt. Express* **2007**, *15*, 14266–14274.
(24) Lippitz, M.; van Dijk, M. A.; Orrit, M. *Nano Lett.* **2005**, *5*, 799.
(25) Danckwerts, M.; Novotny, L. *Phys. Rev. Lett.* **2007**, *98*, 026104.
(26) Talley, C.; Jackson, J.; Oubre, C.; Grady, N.; Hollars, C.; Lane, S.; Huser, T.; Nordlander, P.; Halas, N. *Nano Lett.* **2005**, *5*, 1569–1574.
(27) Romero, I.; Aizpurua, J.; Bryant, G. W.; de Abajo, F. J. G. *Opt. Express* **1993**, *14*, 9988.
(28) Beversluis, M. R.; Bouhelier, A.; Novotny, L. *Phys. Rev. B* **2003**, *68*, 115433.
(29) Lyon, J. L.; Eisele, D. M.; Kirstein, S.; Rabe, J. P.; Bout, D. A. V.; Stevenson, K. J. *J. Phys. Chem. C* **2008**, *112*, 1260–1268.

NL901986G